THE INTERNATIONAL JOURNAL OF MEDICAL ROBOTICS AND COMPUTER ASSISTED SURGERY
Int J Med Robotics Comput Assist Surg 2009; **5**: 444–451.
Published online 1 September 2009 in Wiley InterScience (www.interscience.wiley.com). **DOI:** 10.1002/rcs.276

ORIGINAL ARTICLE

Mechanical analysis of end-to-end silk-sutured anastomosis for robot-assisted surgery

Ying Liu[1]
Shuxin Wang[1]*
S. Jack Hu[2]
Wei Qiu[1]

[1]*School of Mechanical Engineering, Tianjin University, Tianjin 300072, People's Republic of China*

[2]*Department of Mechanical Engineering, University of Michigan, Ann Arbor, MI 48109-2125, USA*

*Correspondence to: Shuxin Wang, School of Mechanical Engineering, Tianjin University, Tianjin 300072, People's Republic of China. E-mail: shuxinw@tju.edu.cn

Accepted: 18 June 2009

Abstract

Background Robot-assisted anastomosis holds great promise for the future. To secure surgery quality, some key process factors, such as the force arrangement of sutures, should be provided because of the lack of haptic feedback in robotics systems

Methods A model of anastomosis is presented to establish the mechanical relationship between vessel and sutures. Stress distribution of the vessel loaded by the suture was then achieved through finite-element simulations, based on the material property test results. Further, experiments were performed to validate the reliability of the FEM simulation of the anastomosis process.

Results To avoid blood osmosis, the allowable lower limit of the suture tension was 0.05 N. To keep the tissue free from injury, the allowable upper limit of tension on the suture was 0.4 N.

Conclusions The study provided meaningful results for directing the robot-assisted anastomosis procedure and design of the surgical tools. Copyright © 2009 John Wiley & Sons, Ltd.

Keywords robot-assisted surgery; surgery simulation; vessel anastomosis; surgery quality; process factor

Introduction

Robot-assisted surgery technology, which is an interdisciplinary field of medicine, biomechanics, mechanics and computer and robotics technology, has become an active research area in recent years. It aims to provide surgeons with tools that enhance and complement their free-hand abilities during surgery. It can not only extend the ability of the surgeon but also enhance the quality of the surgery (1–4). The superiority of robot-assisted surgery lies in the precision and accuracy of surgery by scaling down motion and filtering out hand tremor, and especially the ability to use copious, detailed and diverse information. However, some of the major drawbacks of currently available robotic systems in comparison with free-hand surgery include the lack of haptic feedback and a high degree of hand–eye coordination and judgement, as well as poor adaptability and flexibility.

The lack of haptic feedback limits the effectiveness of operations and may increase tissue trauma, since the surgeon cannot feel the tissue and evaluate the anatomical structures. The force applied to organic tissue can only be estimated through visual feedback by observing the deformation of the tissue (5). Researchers are seeking feasible solutions to tissue manipulation

by adding force measurement and feedback to robotic systems (6–14) and designing instruments to identify tissue propertiues (15–19). Such attempts are still not sufficient to enhance the quality of actual operations, due to a lack of the specific or excessive force applied on the end effectors needed in surgical operations. As such, a force range of end effectors should be specified in robot-assisted surgery.

In addition, robots cannot use qualitative information and efficiently exercise judgement, since they do not possess the hand–eye coordination of human operators. Nevertheless, a robotic system can provide quantitative information of tissue dimensions and deformation and supply force feedback and models of the tissue–instrument interaction to surgeons in robot-assisted surgery (20). Accordingly, detailed commands or preoperative planning systems must be provided to direct a surgical robotic system (21). A general understanding of the surgery process and the relationship between process factors and the quality of surgery are therefore required to complete such manipulations.

This paper studies vessel anastomosis as a specific example of robot-assisted surgery. Vessel anastomosis is one of the most essential and difficult tasks in surgery, but is required in many surgical procedures involving blood vessels. Unfortunately, quite often the quality of the vessel anastomosis is not very satisfactory and may decrease significantly over time. Consequently, many researchers seek approaches to ensure the quality of anastomosis by adjusting the appropriate values of process variables (22–27). However, most of them focus on the wall shear stress distribution that may induce intimal hyperplasia and thrombosis, hence ultimate failure in anastomosis. Little research exists concerning the physical process and prerequisites for a successful anastomosis. Gasser *et al*. (28) first investigated the mechanics of arterial clamping by the finite element method and presented the deformation process of a clamped artery during the artery operation. Schajer *et al*. (29) illustrated how the nonlinear elastic behaviour of artery wall material can cause unusual structural characteristics, using a cross-sectional model of a circular flange of artery material.

This study investigated the physical process of anastomosis, and the force range of sutures in robot-assisted anastomosis surgery is presented here. A mechanical model was used to analyse the suture force and tension loaded on a vessel during the process of end-to-end anastomosis. A three-dimensional (3D) finite element model was developed to analyse the deformation of the tissue and gain stress distribution on the vessel wall. A rubber material was used to simulate the performance of the vessel. Two experiments are also carried out; one was a uniaxial tensile test, used to obtain the constitutive equation of the rubber which was used in place of a vessel in the vessel anastomosis model. The other was a tensile experiment of a rubber/suture structure, used to validate the FEM simulations.

The remainder of the paper is organized as follows. The next section analyses the clinical requirements of end-to-end anastomosis, carries out a material property test to identify the constitutive equation of the rubber used in anastomosis model, and sets up a mechanical model to describe the relationship between the vessel and sutures and a finite element model to gain the wall stress distribution of the vessel. We then present the results of FE simulation and determine the minimal and maximal allowable tension loaded on a vessel through the mechanical model in the process of end-to-end vessel anastomosis.

Materials and Methods

Anastomosis process

The vessel anastomosis technique consists of end-to-end, end-to-side and side-to-side joining (30). The end-to-end anastomosis of equal vessels is relatively simple. This study uses such an anastomosis as an example to investigate the relationship between the quality and process factors in anastomosis. Based on observations of manual anastomosis operations, an anastomosis process can be decomposed into five surgical tasks: vessel exposure and mobilization, create a transverse arteriotomy excision, vessel dilatation and suturing (31,32). The suturing task can be subdivided into the following five steps: stitching, creating a suture loop, developing a knot, placing the knot and securing the knot (33). This paper focuses on the final step of suturing in anastomosis operation: securing a knot, which involves applying a proper tension without injuring the soft tissue or loosening the knot.

In anastomosis operations, several requirements must be met. The surgeon needs to decide the proper type of instruments, the correct positions to entrance bites on the vessel wall, and the exact number of knots according to the diameter and wall thickness of the vessel. It is also required that the knots be placed on the circumference of the vessel by proportional spacing, so that the wall stress is uniform after anastomosis. Therefore, the parameters involved in the process of end-to-end vessel anastomosis are vessel diameter, vessel wall thickness, physical properties of the vessel, diameter of needle, diameter of suture, physical properties of the suture, distance between entry point and cross-section, and number of knots. Since knots are usually placed symmetrically and the same operation is used for every knot, this paper studies only one knot, assuming that all knots are performed the same way.

The basic clinical requirements for a successful anastomosis procedure include: (a) no breaking of thread material; (b) no tissue injury and strangulated sutures; (c) no blood leak; (d) including an equal amount of vessel on the two ends of the divided vessel; and (e) including the entire thickness of the vessel wall and achieving intima-to-intima coaptation. In anastomosis, if the tissue wall stress caused by the tension loaded on the suture is too large, the tissue would be mildly or even severely

DOI: 10.1002/rcs

damaged with wall disruptions. On the other hand, blood would infiltrate from the cross-section of anastomosis if the wall stress is too small. Therefore, the wall stress induced by the tension of the suture must be in an effective range ($[\sigma_{\min}]$, $[\sigma_{\max}]$), where $[\sigma_{\min}]$ is the allowable lower limit of wall stress to avoid blood osmosis and $[\sigma_{\max}]$ is the allowable upper limit of wall stress to prevent injury to the tissue. Consequently, the tension loaded on a suture must be in a corresponding range of ($[T_{\min}]$, $[T_{\max}]$), where $[T_{\min}]$ is the allowable lower limit and $[T_{\max}]$ is the allowable upper limit. Since it is currently technically difficult to precisely control the tension with surgical robotic instruments, tissue wall stress is utilized in this paper as the criterion to estimate the anastomosis quality and the tension loaded on the suture in robot-assisted vessel anastomosis. When suturing the vessels, every stitch should include an equal amount of tissue on the two vessels, include the entire thickness of the vessel wall to achieve intima-to-intima coaptation. These requirements, especially the intima-to-intima coaptation, are decided by the experience and skills of the surgeon, which is not within the scope of this paper.

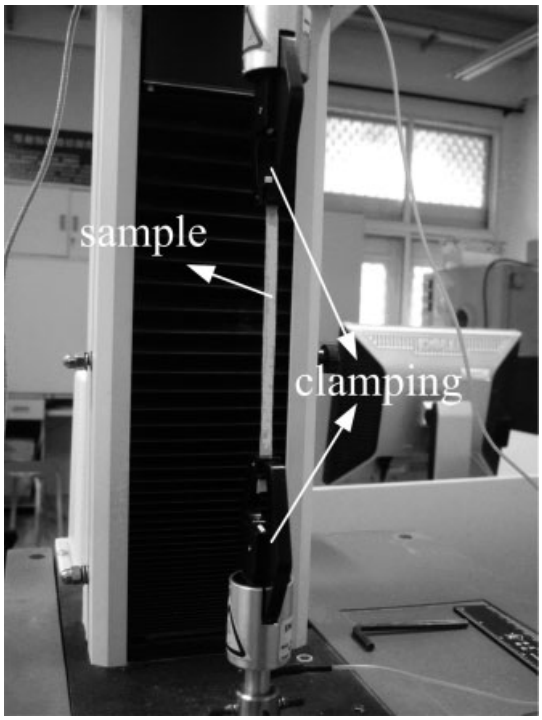

Figure 1. Material test set-up

Material property tests

In this work, the vascular tissue is simulated by a latex rubber used in medical gloves, since the vascular tissue is rubber-like in its mechanical behaviour (34). The rubber describes well the mechanical behaviours and properties of vascular tissue, including the constitutive relationship and damage criteria. Although the viscoelastic characteristics of the real tissue are not included, the plastic failure is well simulated. A uniaxial tensile test is conducted to obtain the stress–strain curve of the latex rubber. The testing machine used is INSTRON-3340 (measuring range, −10 to +10 N). The experimental set-up is shown in Figure 1.

Due to its geometrical and material non-linearities, the mechanical behaviours of rubber materials could not be represented by parameters such as Young's modulus and the Poisson ratio. Therefore, the strain energy function of Marlow (35) was introduced to describe the constitutive relationship of the latex rubber. As shown in Figure 2, the Marlow model is stable in the whole strain range, and the stress–strain curve fitted by the Marlow strain energy function is consistent with the experimental data obtained through a quasi-static uniaxial tensile test, which validates the feasibility of such a model in describing the distortion characteristics of rubber. Hence, the Marlow strain energy function is selected as the constitutive equation of the rubber in the FEM simulation.

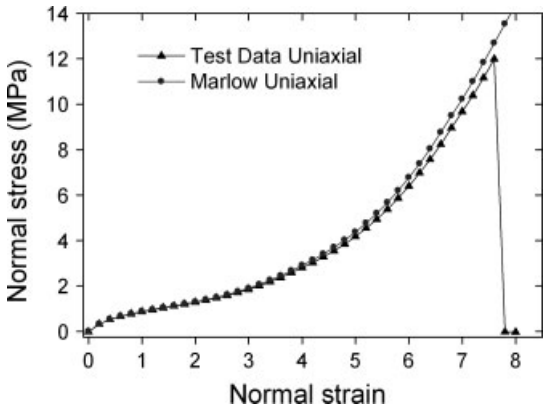

Figure 2. Comparison of uniaxial tensile test data and Marlow model

Mechanical model

After a knot is formed, it is secured by applying the proper tension. For the knot technique, a simple knot is placed on the wound surface by the first throw. The tension loaded onto the suture should be large enough to produce adequate traction force to fix the tissue but not so large as to injure the tissue. The other throws are required be done in the opposite direction. Precise tension should also be applied without breaking or loosening the knot. In this paper, only the first throw is analysed.

Figure 3a shows the force loaded on the suture in the first throw for an end-to-end anastomosis between two equal vessels. Let point p_a be the entry point and p_b the exit point of the suture, respectively. Let F_{1a} be the force of the loop end loaded by the end effector, F_{1b} be the force of the loop end loaded by the vessel tissue, F_{2a} be the force of the post end loaded by the end effector, and F_{2b} be the force of the post end loaded by the vessel tissue. After the needle is drawn through the tissue, the loop end, which holds the needle, is at the exit point p_b and the post end is at p_a. For the first throw, the directions of F_{1a} and

DOI: 10.1002/rcs

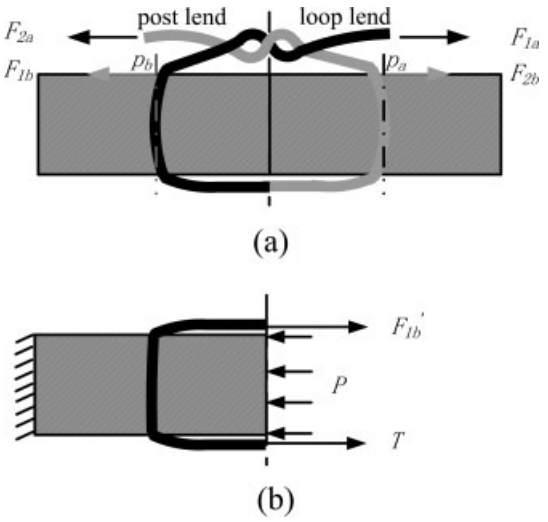

Figure 3. Mechanical model of vessel anastomosis: (a) force analysis of the suture in the first throw; (b) force analysis of vessel tissue on anastomosis cross-section

F_{2a} are required to be opposite and parallel to the axis of the vessel. According to equilibrium, $\sum \vec{F} = 0$, then:

$$\vec{F}_{1a} + \vec{F}_{2a} + \vec{F}_{1b} + \vec{F}_{2b} = 0 \quad (1)$$

$$F_{1a} = F_{2a} \quad (2)$$

$$F_{1b} = F_{2b} \quad (3)$$

A schematic force analysis of the vessel tissue at the cross-section of the end-to-end anastomosis after suturing is conducted as shown in Figure 3b, where T is the tension of the suture, F_{1b}' is the reaction force of F_{1b}, and P is the contact pressure. The suture tension is regarded to be the same everywhere, because the vessel wall is very thin and the interface resistance pressure can be therefore neglected. It is parallel to the axis of the vessel as a result of the flexibility of the suture. Hence:

$$T = F_{1b}' \quad (4)$$

and the total tension of vessel tissue loaded by the single knot is:

$$T_{total} = 2T \quad (5)$$

Since the vessel tissue produces wall stress under suture tension, F_{1b} and F_{2b} should be controlled to a certain range by the medical robotic system. As stated in Anastomosis process, the wall stress must be in an effective range ($[\sigma_{\min}]$, $[\sigma_{\max}]$) and the tension of the vessel tissue loaded by the suture lies in a corresponding range ($[T_{\min}]$, $[T_{\max}]$). The magnitude and distribution of the wall stress of the vessel tissue under the tension, as well as ($[\sigma_{\min}]$, $[\sigma_{\max}]$) and ($[T_{\min}]$, $[T_{\max}]$), are obtained on condition that the anastomosis operation is performed successfully.

FEM model

Vessel tissues undergo large deformation in anastomosis operations. The wall stress of such non-linear biomaterial can be analysed by physical experiments, analytical solutions or numerical analysis. However, the results of existing experimental studies do not provide 3D stress–strain distributions in the vessel wall. In addition, the complexity of the constitutive equation and the non-linearity of the biomaterial prevent analytical solutions. In this paper, finite element numerical analyses are used to obtain the magnitude and distribution of wall stress of vessel tissue, ($[\sigma_{\min}]$, $[\sigma_{\max}]$), and suture tension, ($[T_{\min}]$, $[T_{\max}]$).

According to Patel (36), vascular tissue is rubber-like in its mechanical behaviour and has general properties as follows: homogeneity, incompressibility, orthotropy, non-linearity, incremental linearity, cylindricality and thinness of the vessel wall. The two vascular vessels in an anastomosis operation are physically modelled as cylinders in shape. To simplify the analysis, both vascular cylinders are assumed to be axisymmetric and have the same uniform, thin-walled cross-section. It is also assumed that the initial residual stresses of vascular tissues do not significantly influence the physiological deformations, and the visco-elastic behaviour of the vascular tissue is neglected.

The diameter of the vessel is 4 mm. The thickness of the vascular wall is about 7–12% of vascular diameter, according to Fung (37), hence 0.28–0.48 mm. The distance between the entry point and the cross-section is about the same as the thicknesses of the vascular wall (30–32). The knots are axisymmetric on the circumference of the vessel. The number of knots is about four to twelve, determined by the diameter of the vessel. Accordingly, eight knots will be placed on the vessel. The distance between the cross-section and clamping is about 10 mm.

According to the diameter of the vessel, the type and size of the suture is selected as prolene 7-0 and the type of needle is 7-0. Parameters of the suture and needle are provided in Table 1. According to the tensile strength of the suture, the range of tension loaded on the suture is (0, 1.3) N. Parameters in the anastomosis model are shown in Table 2.

The vessel anastomosis processes are simulated using ABAQUS (35). The FE simulation of the vessel anastomosis process indicates the magnitude and the precise locations of strains and stresses in the structure caused by the applied tension on the suture. Meshes of varying density can be generated in different parts of vessel with desired accuracy and efficiency. The element type selected is C3D8R, an eight-node linear

Table 1. Parameters of suture and needle

Parameter		Value
Suture	Diameter	0.07 (0.05) mm
	Tensile strength	1.37 N
	Density	900 kg/m^3
	Young's modulus	1.32–1.42 GPa
	Poisson ratio	0.35
Needle	Diameter	0.05 mm

DOI: 10.1002/rcs

Table 2. Parameters in the anastomosis model

Parameter	Value
Vessel diameter	4 mm
Vessel thickness	0.4 mm
Distance between entry point and cross-section	0.4 mm
Number of knots	8
Distance between clamping and cross-section	10 mm
Suture	Prolene 7-0
Needle	7-0
Tension loaded on suture	0-1.3 N

brick, isoparametric hexahedral elements with reduced integration and hourglass control. The mesh consists of 151 480 3D elements. The suture tension that affects the quality of vessel anastomosis is obtained by the simulation.

Validation of FEM model

In order to validate the FEM model of vessel anastomosis, a tensile experiment is conducted to describe the tightening process that tightens the suture to join the two vessels together. A rubber sample is loaded by a suture in both the physical and the simulation experiments. The properties of the rubber and the element type used in vessel anastomosis are also selected in these validation experiments. Figure 4 is a schematic of the tensile experiment. Due to the axisymmetric distribution of knots on the circumference of the vessel, the samples used in the tensile experiment are one-eighth of a vessel. Since the thickness of a vessel wall is a fraction of the vessel diameter, the one-eighth thin-walled cylinder is replaced by a rectangular strip with a width of one-eighth of the vessel circumference and the same length as in the anastomosis model. The physical experiment is performed on an INSTRON-3340 tensile testing machine with a measuring range of −10 to +10 N.

The same parameters are used in the FEM simulation as those in the physical experiments. The C3D8R elements

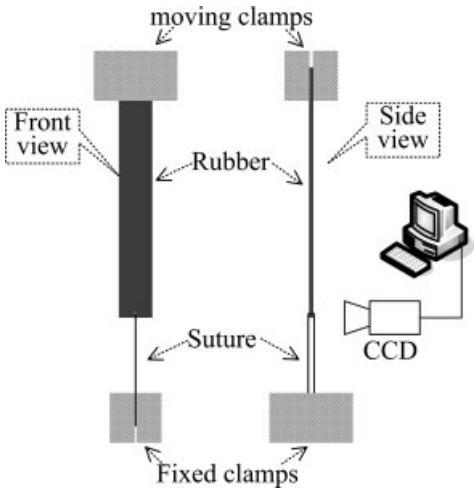

Figure 4. Schematic tensile experiment of rubber–suture structure

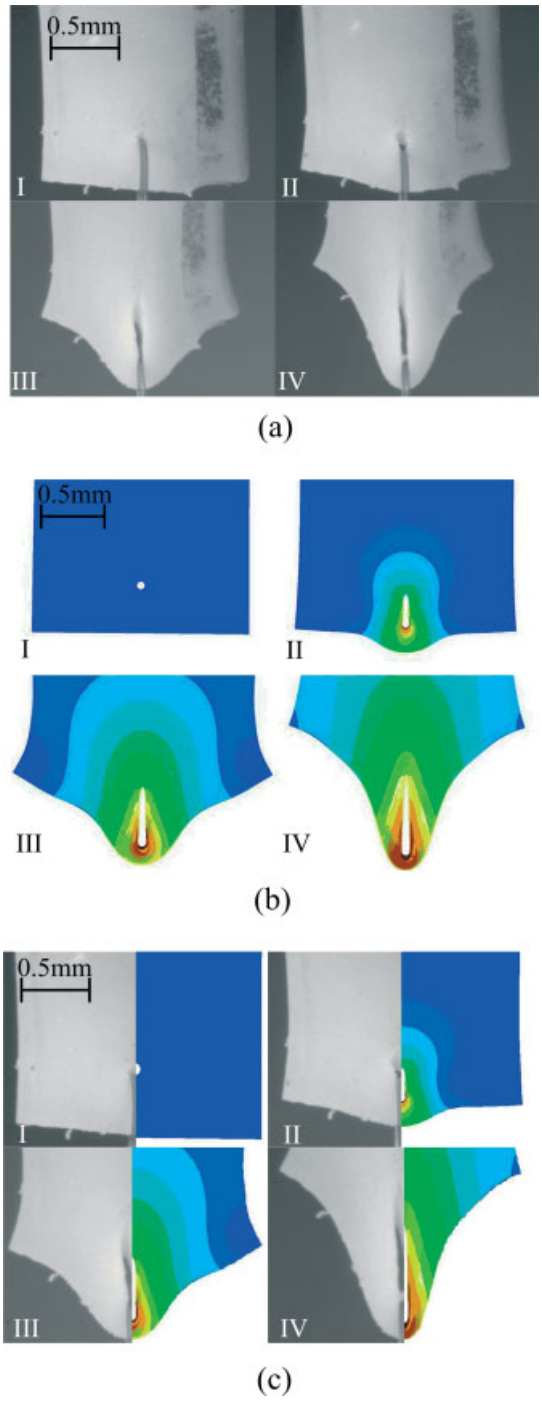

Figure 5. Physical experiment and FEM simulation of tissue deformation: (a) tissue deformation in the physical experiment; (b) tissue deformation predicted via FEM simulation; (c) comparisons of tissue deformation between the physical experiment and the FEM simulation

are used to model the vessels. The mesh consists of 75 480 3D elements. Deformation of the polysulphide rubber and needle hole was observed in the tensile experiment when the samples are pulled by sutures. Figure 5a shows the deformation of the tissue and needle hole during the tightening process in a physical experiment. The tissue deformations are illustrated when the force loaded on the suture is 0, 0.05, 0.1 and 0.2 N, respectively. Figure 5b

is the corresponding FEM simulation result. The physical experiment results are consistent with FEM simulation results, as shown in Figure 5c. This validates the reliability of FEM simulation of the vessel anastomosis process.

Results

This section presents the FEM simulation results of vessel anastomosis, the allowable load range that avoids the blood leakage and keeps the vessel free from tissue injury.

Deformed states of vessel at different load levels

The deformed states of the vessel before and after the suture tension are illustrated in Figure 6. By taking advantage of the symmetry, the vessel deformation is demonstrated by only one-eighth of the whole body. As can be seen from Figure 6, the region affected by the suture tension is relatively small and focuses on the area around the needle hole. Figure 7 illustrates the vessel near the needle hole in different deformed states during the anastomosing process; Figure 7a represents the physiological configuration before the suture tension, while Figure 7b–d shows the vessel deformation when the tension loaded on suture is 0.05, 0.2 and 0.3 N, respectively.

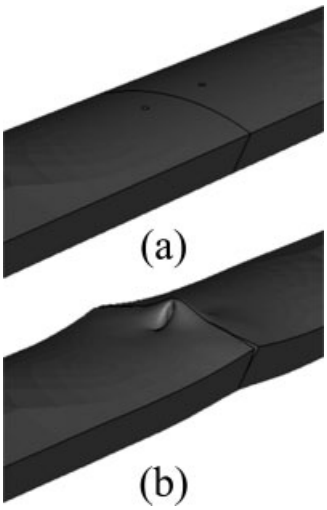

Figure 6. Deformed states of a vessel before (a) and after (b) anastomosis

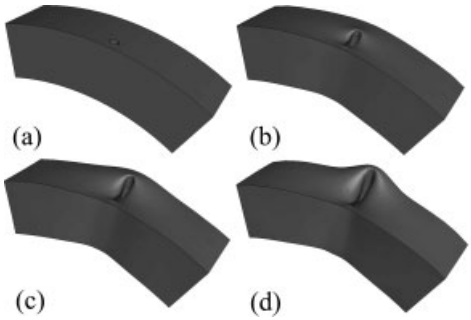

Figure 7. Deformed states of a vessel around the needle hole at different suture tensions: (a) physiological configuration before the suture tension is loaded; (b) suture tension load of 0.05 N; (c) tension load of 0.2 N; and (d) tension load of 0.3 N

Stress distribution of vessel

Figure 8 shows the wall stress distribution of the tissue near the needle hole when the tension loaded by suture is 0.4 N. As can be seen from Figure 8a, the stress is symmetrically distributed and decreases from the middle to the side on transverse section of the two vessels. There is also a tendency for the longitudinal stresses to decrease from the inner wall to the outer wall. From Figure 8b, we can see that the tissue around the needle hole protrudes and the circular shape of the needle hole becomes elliptical. The long axis of the ellipse is parallel to the axis of the vessel and the minor axis is parallel to the cross-section of the vessel. The maximal stress of tissue occurs in the bilateral area in the neighborhood of the needle hole near the cross-section from the stress distribution in Figure 8c.

Effective range of tissue stress and suture tension

From the vessel wall stress distribution on the transverse section, blood leakage initially occurs in the middle of the two knots on the inner wall of the transverse section after the anastomosis is completed. For convenience, the distribution of longitudinal stress on the inner wall of the transverse section can be presented by the curve in Figure 9. σ_1 is the longitudinal stress on the sides and σ_2 is the longitudinal stress on the middle. To avoid blood leakage from the transverse section, the longitudinal stress

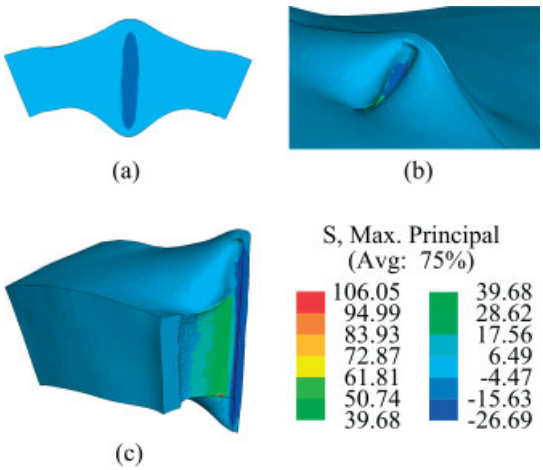

Figure 8. Tissue stress distribution: (a) stress distribution in a transverse section of the two vessels; (b) stress distribution on the two segments of vessel around the needle hole; and (c) stress distribution on a cross-section parallel to the axis of the vessel

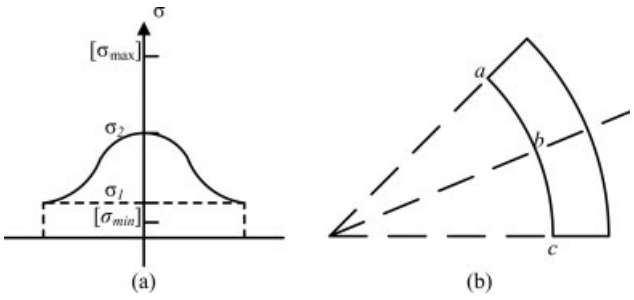

Figure 9. Distribution of longitudinal stress on the inner wall of a transverse section: (a) distribution curve of longitudinal stress; (b) transverse section of vessel, in which σ_1 is the longitudinal stress at points *a* and *c* and σ_2 is the longitudinal stress at point *b*

induced by the suture tension must be greater than that at normal blood pressure.

According to (36,38), circumferential, longitudinal and radial stresses are the dominant stresses in the vessel wall under physiological conditions when blood flows in a blood vessel. At normal blood pressure, the circumferential stress is of the order of 10^5 Pa, which is generally tensile. The longitudinal stress is smaller but of the same order of magnitude, and also usually tensile. The radial stress is an order of magnitude smaller and is usually compressive stress. So the longitudinal stress (0.1 MPa) (38) at the normal blood is selected as $[\sigma_{\min}]$. Table 3 shows the simulation results of tissue wall stress when the tension loaded on the suture reaches 0.05 N. It can be concluded from Table 3 that the blood would not flow out from the anastomosis section when the tension loaded on the suture reaches 0.05 N.

Another great failure in operation of vessel anastomosis is tissue ripping. For rubber-like materials that generally fail due to plastic deformation, damage criteria include limiting stress and energy degradation. In this study, limiting stress was selected as $[\sigma_{\max}]$, the damage criterion for vessel trauma. The limiting stress of tissue obtained from the material testing was 106.05 MPa. The maximum principal stress of tissue (σ_3) extracted from the FEM simulation results is used as the evaluation indicator of tissue damage. The vessel begins to produce cracks when σ_3 exceeds $[\sigma_{\max}]$. It can be concluded from the simulation results that the maximum principal stress of tissue reaches $[\sigma_{\max}]$ when the tension of the suture (T) reaches 0.4 N.

Hence, the effective arrangement of suture tension is (0.05 N, 0.4 N) to perform the anastomosis without blood leakage and tissue ripping simultaneously. This is in accordance with the results of Kitagawa (39), who measured the normal range of tension applied on sutures during the first throw of a knot.

Table 3. Wall stress of tissue when suture tension was 0.05 N

Parameter	Value
Circumferential stress	−0.144 MPa
Longitudinal stress	−0.108 MPa
Radial stress	0.03 MPa

Discussion

Vessel anastomosis is a mechanical procedure, and a mechanical model is required to study the effects of the suture force on anastomosis quality in robot-assisted surgery. In this study, the influence of suture force on the quality of end-to-end anastomosis was investigated for the first time, using the finite element method and physical experiments. The proposed approach was determination of the allowable range of tension loaded on the suture, which has a major influence on the distribution of tissue stresses. The model and experimental results demonstrate that the mechanical model allows a detailed study of anastomosis procedures. The simulated 3D deformations perfectly resemble the typical shape of the vessel tissue around the needle hole. Stress analysis reveals that the tissue stress is larger during vessel tightening than during knot securing, even when the force loaded on the suture is the same. Hence, tissue damage mostly happens at the stage of tightening, rather than of knot securing. Based on the experimental results, the allowable lower limit of suture tension to avoid blood osmosis is 0.05 N, and the allowable upper limit loaded on the suture to keep the tissue free from ripping is 0.4 N. This is the first time that the force range of end-to-end anastomosis has been quantitatively investigated. The meaningful results obtained can be used to guide surgical procedure and to design surgical tools to improve the quality of end-to-end anastomosis in robot-assisted surgery. For example, the surgeon could use more caution when tightening the suture, since the tissue damage mostly happens at this step of the operation. Based on the allowable load range ($[T_{\min}]$, $[T_{\max}]$), the traction force of the needle and the clamping force of the end-effector can be obtained additionally, according to the equation of equilibrium for the knot tying model (40). This provides a basis in strength calculation for the design of surgical tools.

Acknowledgements

This research was supported by the National High-Tech R&D Programme of China (863 Programme; Grant No. 2007AA04Z247), the NSFC (Grant No. 50575162), the Tianjin Municipal Science and Technology Development Programme (Grant No. 07JCZDJC09000) and National Natural Science Funds for Distinguished Young Scholar.

References

1. Speich JE, Rosen J. Medical robotics. In *Encyclopedia of Biomaterials and Biomedical Engineering*, Bowlin GL, Wnek G (eds). Marcel Dekker: New York, 2004; 983–993.
2. Zamorano L, Li Q, Jain S, Kaur G. Robotics in neurosurgery: state of the art and future technological challenges. *Int J Med Robot Comp* 2004; **1**(1): 7–22.

3. Belsley SJ, Byer A, Ballantyne GH. MIRA and the future of surgical robotics. *Int J Med Robot Comp* 2006; **2**(1): 98–103.
4. Cleary K, Nguyen C. State of the art in surgical robotics: clinical applications and technology challenges. *Comput Aided Surg* 2001; **6**(6): 312–328.
5. Puangmali P, Althoefer K, Seneviratne LD, *et al*. State-of-the-art in force and tactile sensing for minimally invasive surgery. *IEEE Sens J* 2008; **8**(3–4): 371–381.
6. Nagy I, Mayer H, Knoll A, *et al*. The Endo(PA)R system for minimally invasive robotic surgery. Proceedings of the IEEE/RSJ International Conference on Intelligent Robots and Systems, Sendal, Japan, 28 September–2 October 2004; 3637–3642.
7. Ye D, Mozaffari-Naeini H, Busart C, *et al*. MEMSurgery: an integrated test-bed for vascular surgery. *Int J Med Robot Comput* 2005; **1**(3): 21–30.
8. Tavakoli M, Patel RV, Moallem M. A haptic interface for computer-integrated endoscopic surgery and training. *Virtual Real* 2006; **9**(2–3): 160–176.
9. Kim K, Chung WK, Nam SY. Accurate force reflection method for a multi-DoF haptic interface using instantaneous restriction space without a force sensor in an unstructured environment. *Adv Robotics* 2007; **21**(1–2): 87–104.
10. Shimachi S, Hirunyanitiwatna S, Fujiwara Y, *et al*. Adapter for contact force sensing of the da Vinci® robot. *Int J Med Robot Comp* 2008; **4**(2): 121–130.
11. Her MG, Hsu KS, Lan TS, *et al*. Haptic direct-drive robot control scheme in virtual reality. *J Intell Robot Syst* 2002; **35**(3): 247–264.
12. Preusche C, Hirzinger G. Haptics in telerobotics – current and future research and applications. *Visual Comput* 2007; **23**(4): 273–284.
13. Katsura S, Iida W, Ohnishi K. Medical mechatronics – an application to haptic forceps. *Annu Rev Control* 2005; **29**(2): 237–245.
14. Wang S, Ding J, Yun J, *et al*. A robotic system with force feedback for microsurgery. Proceedings of the 2005 IEEE International Conference on Robotics and Automation, Barcelona, Spain, April 2005; 199–204.
15. Samur E, Sedef M, Basdogan C, *et al*. A robotic indenter for minimally invasive characterization of soft tissues. *Int Congr Ser* 2005; **1281**: 713–718.
16. Brown JD, Rosen J, Kim YS, *et al*. *In vivo* and *in situ* compressive properties of porcine abdominal soft tissues. *Med Meets Virtual Real* 2003; **94**: 26–32.
17. Menciassi A, Eisinberg A, Carrozza MC, *et al*. Force sensing microinstrument for measuring tissue properties and pulse in microsurgery. *IEEE–ASME Trans Mech* 2003; **8**(1): 10–17.
18. Noonan DP, Liu H, Zweiri YH, *et al*. A dual-function wheeled probe for tissue viscoelastic property identification during minimally invasive surgery, IEEE International Conference on Robotics and Automation, Rome, Italy, 10–14 April 2007; 2629–2634.
19. Bicchi A, Scilingo EP, Rossi DD. Haptic discrimination of softness in teleoperation: the role of the contact area spread rate. *IEEE Trans Robotic Autom* 2000; **16**(5): 496–504.
20. Stallkamp J, Schraft RD. A technical challenge for robot-assisted minimally invasive surgery: precision surgery on soft tissue. *Int J Med Robot Comp* 2005; **1**(2): 48–52.
21. Howe RD, Matsuoka Y. Robotics for surgery. *Annu Rev Biomed Eng* 1999; **1**: 211–240.
22. Weston MW, Rhee K, Tarbell JM. Compliance and diameter mismatch affect the wall shear rate distribution near an end-to-end anastomosis. *J Biomech* 1996; **29**(20): 187–198.
23. Zidi M, Cheref M. Mechanical analysis of a prototype of small diameter vascular prosthesis: numerical simulations. *Comput Biol Med* 2003; **33**(1): 65–75.
24. Al-Sukhun J, Lindqvist C, Ashammakhi N, *et al*. Microvascular stress analysis – Part I: simulation of microvascular anastomoses using finite element analysis. *Br J Oral Max Surg* 2007; **45**(2): 130–137.
25. Longest PW, Kleinstreuer C, Deanda A. Numerical simulation of wall shear stress and particle-based hemodynamic parameters in pre-cuffed and streamlined end-to-side anastomoses. *Ann Biomed Eng* 2005; **33**(12): 1752–1766.
26. Hofer M, Rappitsch G, Perktold K, *et al*. Numerical study of wall mechanics and fluid dynamics in end-to-side anastomoses and correlation to intimal hyperplasia. *J Mech* 1996; **29**(10): 1297–1308.
27. Keynton RS, Evancho MM, Sims RL, *et al*. The effect of graft caliber upon wall shear within *in vivo* distal vascular anastomoses. *J Biomech Eng–Trans ASME* 1999; **121**(1): 79–88.
28. Gasser TC, Schulze-Bauer CAJ, Holzapfel GA. A three-dimensional finite element model for arterial clamping. *J Biomech Eng–Trans ASME* 2002; **124**(4): 355–363.
29. Schajer GS, Green SI, Davis AP, *et al*. Influence of elastic nonlinearity on arterial anastomotic compliance. *J Biomech Eng–Trans ASME* 1996; **118**(4): 445–451.
30. Ascher E, Hollier LH, Strandness DE Jr, *et al*. *Haimovici's Vascular Surgery*. Wiley-Blackwell: Chichester, 2003.
31. Liu X. *Histology and Embryology*. People's Medical Publishing House: Beijing, 1994.
32. Guo W, Xu M. *Basic Surgical Operation*. Scientific and Technical Documents Publishing House: Beijing; 1993.
33. Kang H, Wen JT. Robotic knot tying in minimally invasive surgery. Proceedings of the IEEE/RSJ International Conference on Intelligent Robots and Systems, Lausanne, Switzerland, October 2002; 1421–1426.
34. Wagner CR, Stylopoulos N, Howe RD. The role of force feedback in surgery: analysis of blunt dissection. 10th Symposium on Haptic Interfaces for Virtual Environment and Teleoperator Systems, Orlando, FL, 24–25 March 2002; 68–74.
35. ABAQUS Theory Manual. Hibbitt,Karlsson & Sorensen Inc: http://www.simulia.com/support/documentation.html.
36. Patel DJ, Vaishnav RN. *Basic Hemodynamics and Its Role in Disease Processes*. University Park Press: Baltimore, MD, 1980.
37. Fung YC. *Biomechanics: Mechanical Properties of Living Tissues*. Springer-Verlag: Berlin, 1983.
38. Fung YC. *Biomechanics: Motion, Flow, Stress, and Growth*. Springer-Verlag: New York, 1990.
39. Kitagawa M, Okamura AM, Bethea BT, *et al*. Analysis of suture manipulation forces for teleoperation with force feedback. Proceedings of the Fifth International Conference on Medical Image Computing and Computer Assisted Intervention – MICCAI 2002. *Lect Notes Comput Sci* 2002; **2488**: 155–162.
40. Yue L, Wang S, Zeng Y, *et al*. Analysis of virtual vessel suture based on multi-body theory. *J Tianjin Univ* 2006; **39**(1): 89–95.